Journal of Photochemistry and Photobiology A: Chemistry 208 (2009) 27–35

Contents lists available at ScienceDirect

Journal of Photochemistry and Photobiology A: Chemistry

journal homepage: www.elsevier.com/locate/jphotochem

Photoelectrocatalytic degradation of ethylene by a combination of TiO_2 and activated carbon felts

Sheng-ying Ye*, Qing-mei Tian, Xian-liang Song, Shu-can Luo

College of Food Science, South China Agricultural University, Wushan, Guangzhou, GD 510640, PR China

ARTICLE INFO

Article history:
Received 30 October 2008
Received in revised form 21 March 2009
Accepted 4 August 2009
Available online 12 August 2009

Keywords:
Ethylene
Photoelectrocatalytic
Titanium dioxide
Activated carbon felts
Storage

ABSTRACT

Postharvest loss of quality is an important problem in the food and horticultural product industry. One of the major factors contributing to loss of quality is the uncontrolled exposure of the products to small amounts of ethylene gas during storage. In this study we investigated the photoelectrocatalytic (PEC) degradation of ethylene gas at a temperature of $3 \pm 1\,^{\circ}C$ and relative humidity of $90 \pm 3\%$ on an activated carbon felts (ACF)-supported photocatalyst titanium dioxide photoelectrode [TiO_2/ACF] or on a photoelectrode which had been modified by coating the ACF support with platinum [TiO_2/ACF-Pt]. The apparent pseudo-first-order kinetic model was used to describe the PEC degradation of ethylene. The key designing parameters for a PEC reactor affecting the degradation efficiency in terms of the rate constant of this model were studied, including the bias voltage and the light intensity. Degradation of ethylene by applying a bias voltage to the [TiO_2/ACF] |Nafion|[TiO_2/ACF] electrode-membrane assembly or to the [TiO_2/ACF-Pt] |Nafion|[TiO_2/ACF-Pt] electrode-membrane assembly enhanced the efficiency of photocatalytic (PC) degradation. The combination of the ACF support modified with platinum and the applied bias voltage were found to have an additive enhancement effect on the rate constant compared to PEC degradation carried out using the unmodified ACF support. With respect to the [TiO_2/ACF-Pt] |Nafion|[TiO_2/ACF-Pt] electrode-membrane assembly, a kinetic model was established using response surface methodology to describe the relationship between the rate constant and the affecting parameters. Optimized parameters were found to be a light intensity of 3.1 mW cm^{-2} with a bias voltage of 47.5 V.

1. Introduction

Ethylene gas (C_2H_4) is released by fruit and vegetable and acts as a plant hormone that controls many plant responses [1]. Ethylene gas is beneficially used in many instances such as the promotion of uniform ripening in bananas, and de-greening of fresh citrus. However, the effects of ethylene gas are not all positive. Even small amounts of ethylene gas in the atmosphere in the storage facility can induce undesirable reactions in most fresh produce, such as development of senescence, bitter flavors, chlorophyll loss, disease susceptibility and physiological disorders. Storage of produce is of economic importance to the food and horticultural industries. Storage allows producers, handlers and sellers to spread availability over periods of high and low demand, maintaining supply and stabilizing costs. Within the industry in Guangdong Province, PRC, it is estimated that 30% of losses are directly related to ethylene exposure. Removal of ethylene from the storage environment retards spoilage, reduces loss and increases profit. While conventional methods such as venting, potassium permanganate oxidation, adsorption onto brominated carbon, catalytic oxidizers, and hypobaric storage help to control and remove ethylene from storage facilities, each has limitations in controlling ethylene levels in the presence of high ethylene-yielding produce and can result in the alteration of temperature and humidity conditions in the storage facilities [2].

Photocatalysis (PC) using titanium dioxide (TiO_2) as the catalyst is seen as a promising alternative to the oxidation processes used to degrade ethylene in most conventional methods and has attracted considerable attention over the last 10 or more years [3–6]. Maneerat et al. [7] reported that the photocatalytic degradation of ethylene using TiO_2 can be carried out under high humidity at both room temperature and low temperature. The major advantage of this technology is the complete mineralization of undesirable organic contaminants in gas phases to CO_2 and H_2O in addition to the chemical stability of the catalyst, which is also non-toxic and inexpensive. When TiO_2 is irradiated with ultraviolet (UV) light whose photon energy exceeds 3.2 eV, holes (H^+) and electrons (e^-) are created on the surface of the TiO_2, the former being powerful oxidizing agents and the latter reducing agents. However, recombination of photogenerated holes and electrons (H^+/e^-) occurs at the same time. The high level of recombination between holes and electrons is a major factor contributing to the

* Corresponding author. Tel.: +86 20 85283431.
E-mail address: yesy@scau.edu.cn (S.-y. Ye).

1010-6030/$ – see front matter.
doi:10.1016/j.jphotochem.2009.08.001

reduction in the catalytic ability of TiO_2 and to the control of the PC efficiency [8,9]. In this regard, various attempts have been made to enhance the PC efficiency of TiO_2, such as the photoelectrocatalytic (PEC) oxidation process. In the case of PEC, the PC reaction is further accelerated by applying an external potential which moves the conduction band electrons away from the TiO_2 photo-anode towards a counter electrode [10]. This is an efficient way to prevent the recombination of H^+/e^- pairs and results in extending the life of the active holes [11–13]. There are some reports relating to the PEC process [14–17], but in these studies, the organic contaminants in water or wastewater were used to investigate the PEC degradation.

TiO_2 is mostly frequently applied to a carrier or support before use [18]. The development of a TiO_2 photocatalyst anchored on supporting materials with a large surface area on which ethylene could be condensed would be of great importance in the indoor environment of storage facilities where the ethylene concentration is dilute under conditions of high relative humidity and low temperature. Activated carbon felts (ACF) are especially interesting as potential support materials due to their excellent characteristics and properties. The surface area of these activated carbon felts is very high, and the porous network is mainly formed by deep pores in a narrow range of sizes, especially micropores [19]. This form of activated carbon has important advantages over granular activated carbon, such as, the uniform distribution of microporosity, a superior rate of adsorption and desorption, and a more rapid attainment of equilibrium [20,21]. ACF has been introduced as the support material for TiO_2 in some photocatalysis studies, and the enhancement of gas phase toluene condensation as a result of the combined adsorption of ACF with photocatalysis TiO_2 has been reported [22,23]. Recent studies have reported the modification of ACF by metal doping which has led to the improved removal of specific contaminants in the gas as a result of changes to the physical and chemical properties of the surface of the carbon materials [24,25]. Although the photoelectrocatalytic (PEC) degradation of organic pollutants in liquid phases has been carried out using a TiO_2 film, the PEC degradation of ethylene gas under conditions of high relative humidity and low temperature on an ACF-supported TiO_2 photoelectrode [TiO_2/ACF] or on a photoelectrode consisting of the photocatalyst TiO_2 supported on an ACF support modified with a noble metal [TiO_2/ACF-M] has rarely been reported until now.

Taking into account these findings, we have carried out preliminary work on the photoelectrocatalytic (PEC) degradation of ethylene gas at a temperature of $3 \pm 1\,^{\circ}C$ and relative humidity $90 \pm 3\%$ using an ACF-supported photocatalyst TiO_2 photoelectrode [TiO_2/ACF] or a photoelectrode consisting of the photocatalyst TiO_2 supported on an ACF support modified by the deposition of Platinum [TiO_2/ACF-Pt]. The key designing parameters for a PEC reactor affecting the degradation efficiency in terms of the rate constant were studied, including the bias voltage and the light intensity. A systematic experimental design based on response surface methodology (RSM) was used for modeling and optimization of the designing parameters of PEC reactor. In addition, the surface morphology and elements of electrode have been characterized by scanning electron microscopy (SEM) and X-ray photoelectron spectroscopy (XPS).

2. Materials and methods

2.1. Material

Titanium dioxide used in this study was Degussa P25, which is composed mainly of anatase (ca. 70%) and is composed of non-porous polyhedral particles with a mean size of 30 nm and a surface area of $50\,m^2\,g^{-1}$. Viscose rayon-based ACF (Sutong Carbon Fibers Co. Ltd., Jiangsu Province, China) with a 3-mm thick felt, was chosen as the supporting substrate for TiO_2. The perfluorinated membrane Nafion®324 (DuPont Inc.), reinforced with poly (tetrafluoroethylene) fiber was 0.15 mm thick. Tape 9713 model *XYZ*-Axis Electrically Conductive tape was purchased from 3M Inc.

2.2. Preparation of ACF-supported TiO_2 film and electrode-membrane assembly

An aqueous suspension of TiO_2 ($25\,g\,L^{-1}$) and sodium carboxymethyl cellulose ($0.02\,g\,L^{-1}$) was agitated and sonicated for 30 min. ACF-supported TiO_2 films [TiO_2/ACF] were prepared by dip coating rectangular ACF (40 mm × 40 mm), in the TiO_2 suspension at a withdrawal speed of $0.42\,cm\,s^{-1}$, after coating, the resulting materials were dried at 100 °C for 12 min, and were then calcinated at 200 °C for 1 h using a temperature gradient of 5 °C/min. and cooled to room temperature. The same procedure was followed for loading TiO_2 onto ACF which had initially been coated with Pt using a vacuum ion sputter. The amount of TiO_2 used was determined by the weight difference before and after the dip coating procedure. In all experiments the weight of TiO_2 was $0.67\,g \pm 5\%$. The [TiO_2/ACF] and [TiO_2/ACF-Pt] films act as both catalysts and electrodes.

Nafion®324 was used as the polymer electrolyte membrane. The electrode-membrane assembly (EMA) was fabricated for the experiments by placing two electrodes on either side of the Nafion®324 membrane. Prior to use, the membrane was cleaned in H_2O. Tape 9713 was cut into 3 mm × 3 mm in size and placed at four corners of the Nafion®324 membrane for the fastness between electrode and the membrane. Electrical contact of electrode was achieved with a wire attached to the surface of the films with the conductive adhesive tape.

The surface morphology of the films and TiO_2 particles supported on ACF was examined using a XL30 model Scanning Electron Microscopy (Philips Co, Holland) and a Quanta 400 model Field Emission Scanning Electron Microscope (Philips Co., Holland), respectively. X-ray photoelectron spectroscopy (XPS) was used to characterize the surface elements of the electrode. The data were recorded on an Axis-Ultra-DLD model XPS instrument (Kratos Analytical Ltd., England), using an Al Kα X-ray source (h_γ = 1486.6 eV) for the excitation of electrons. The data were converted into VAMAS file format and imported into a CasaXPS software package for manipulation and curve-fitting.

2.3. PEC reactor system

To simulate conditions inside a produce storage facility, the temperature and relative humidity in all studies were controlled at $3 \pm 1\,^{\circ}C$ and $90 \pm 3\%$, respectively. The apparatus constructed to measure ethylene degradation by PEC is shown schematically in Fig. 1. The PEC reactor system consisted of a cylindrical vessel, UV lamp, a direct current fan, a potentiostat and the EMA. A cylindrical vessel with a volume of 10 L was used. Illumination was provided by 2 W ozone-free double-tube cold cathode UV lamp set at a wavelength of 254 nm (Bright Star Co., China). The UV intensity at the surface of the film can be changed by altering the distance between the lamp and the film, depending on the experimental settings. The light intensity was measured with a Sensor EW97503-50 model UV intensity meter (Cole-Parmer CO, USA). An axial-flow fan was installed to ensure adequate mixing of the air in the vessel. The flow-rate used in all studies was $0.28\,mm^3\,min^{-1}$. A potentiostat (Huatai Co., China, model WYK-10020K) supplied potential bias to the EMA and had a voltage control range of 0–100 V. The EMA; two UV lamps and the fan were mounted on an insulating board of 300 mm × 300 mm in size. All of these elements were placed into a cylindrical vessel so that the gas mixture came into contact with both the electrodes in the assembly.

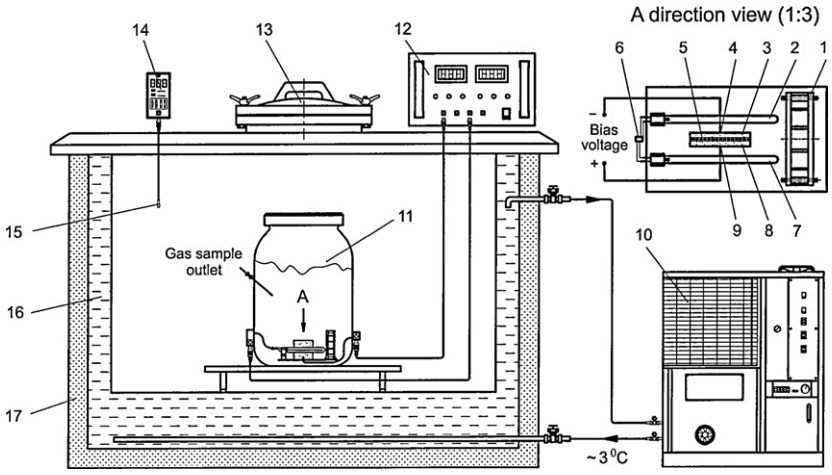

Fig. 1. A Schematic display of the experimental setup. (1) Direct current fan; (2, 7) double-tube UV lamp; (3, 8) TiO_2/ACF or TiO_2/ACF-Pt; (4, 9) electrical conductive tape; (5) Nafion®324; (6) pinboard to UV lamp; (10) refrigerator; (11) cylindrical vessel; (12) potentiostat; (13) airproof handhole; (14) control unit for temperature and relative humidity; (15) sensor; (16) coolant; (17) adiabatic layer.

Prior to a test, pre-exposure of the reactor system to ethylene was achieved by allowing an air–ethylene mixture to enter the system from the inlet and to circulate with the UV lamps and the potentiostat turned off. The system was allowed to settle for 240 min. The purpose of this procedure was to precondition the system in order to counter the adverse effects of ethylene adsorption by the system components which would otherwise interfere with the PEC degradation of ethylene. The adsorption of ethylene by the system was first tested in the absence of UV irradiation, and the results showed that adsorption equilibrium was attained at 240 min. After 240 min, the opening of cylindrical vessel was closed and the UV lamps and the DC power were turned on, the concentration of ethylene was sampled for analysis at 40-min intervals. The initial concentration of ethylene was adjusted to a volume of ~45.5 mg m^{-3}.

2.4. Analytical methods

Quantitative analysis of ethylene was carried out using a model GC-7890II (Techcomp Ltd., China) combined with a computer and appropriate software for data analysis. Teflon syringes (3 mL, gas-tight) were used to sample the ethylene. Surgical septa were used to cap the ends of the syringe needles after the removal of samples and were removed just prior to injection into the gas chromatograph (GC). Operating temperatures for the GC were as follows: oven temperature 45 °C, injector 150 °C, and detector 200 °C. The GC analysis was carried out under isothermal conditions using a 2 m Porapak QS80/100 column (Atech Technologies CO Ltd., China) with a 3 mm inner diameter. Nitrogen was used as the carrier gas and was passed through the GC column at a flow-rate of 26.62 mL min^{-1}; a flame ionization detector (FID) was used to capture and analyze ethylene concentrations. The GC make-up gas was air and hydrogen.

It is well established that photocatalysis experiments follow the Langmuir–Hinshelwood (L–H) model:

$$-\frac{dC}{dt} = \frac{kKC}{1+KC} \tag{1}$$

where k is the reaction rate constant (min^{-1}), K is the adsorption coefficient of the reactant (m^3 mg^{-1}) and C is the reactant concentration (mg m^{-3}). When C is very small, KC is negligible with respect to unity and Eq. (1) describes pseudo-first-order kinetics. Integration of pseudo-first-order kinetics with the limit conditions that at the start of radiation, $t = 0$, the concentration is the initial one, and $C = C_0$, yields Eq. (2)

$$\mathrm{Ln}\left(\frac{C_0}{C_t}\right) = K' t \tag{2}$$

where $K' = kK$ is the apparent pseudo-first-order rate constant (min^{-1}).

For a reaction that follows pseudo-first-order kinetic model, plotting values of $\mathrm{Ln}(C_0/C_t)$ against time would give a straight line, the slope of which would be equal to K'. In this work, pseudo-first-order kinetics was confirmed in both the PE and PEC degradation of ethylene.

2.5. Procedures in the PEC degradation experiment

A total of three sets of experiments was carried out for different purposes and the experimental conditions are summarized in Table 1. The first set of experiments using the [TiO_2/ACF]|Nafion|[TiO_2/ACF] assembly was conducted under the dark (electrochemical, EC), PC and PEC processes, to compare the rate constant (K') of the PEC with that of the PC and EC. The second set of experiments was carried out by applying different electrical biases to the [TiO_2/ACF]|Nafion|[TiO_2/ACF] or [TiO_2/ACF-Pt]|Nafion|[TiO_2/ACF-Pt] assembly to investigate the relationship between electrical bias and the rate constant (K') of the PEC. The third set of experiments used the [TiO_2/ACF-Pt]|Nafion|[TiO_2/ACF-Pt] assembly and was carried out to establish a kinetic model for studying the effect on the K' value of the designing parameters of PEC reactor, a systematic experimental design based on response surface methodology (RSM) was used. Our preliminary studies (data not shown) indicated that the light intensity and applied electrical bias were two major designing parameters of PEC reactor affecting the degradation efficiency, while the flow-rate of axial-flow fan had little effect on it. Therefore, bias voltage (Z_1) and light intensity (Z_2) were included as central composite rotatable design (CCRD) factors. Coded and original levels for independent variables are showed in Table 2.

Using RSM, the quantitative form of the relationship between the desired response and the independent input variables can be represented by Eq. (3):

$$\hat{K}' = f(Z_1, Z_2) \tag{3}$$

where $\hat{K}'$ represents the estimated value of the desired response and f represents the response function (or response surface). In this study, the approximation of $\hat{K}'$ was derived by fitting the data

Table 1
The summary of experimental conditions.

Name of experiment		Membrane-electrode assembly			Electrical bias (V)	Light intensity ($mW\,cm^{-2}$)
		Anode	Electrolyte	Cathode		
1st set	Test1 (Dark)	TiO_2/ACF	Nafion	TiO_2/ACF	82.5	0.0
	Test2 (PC)	TiO_2/ACF	Nafion	TiO_2/ACF	0.0	3.1
	Test3 (PEC)	TiO_2/ACF	Nafion	TiO_2/ACF	82.5	3.1
2nd set	Exp1 (PEC)	TiO_2/ACF	Nafion	TiO_2/ACF	12.5; 30; 47.5; 65; 82.5	3.1
	Exp2 (PEC)	TiO_2/ACF-Pt	Nafion	TiO_2/ACF-Pt	12.5; 30; 47.5; 65; 82.5	3.1
3rd set	RSM (PEC)	TiO_2/ACF-Pt	Nafion	TiO_2/ACF-Pt	12.5; 22.75; 47.5; 72.25; 82.5	0.8; 1.14; 1.95; 2.76; 3.1

Table 2
Central composite design for the modeling of PEC for degradation of ethylene.

Run no.[a]	Independent variables		Response variable[b]
	Bias voltage (V) (Z_1)	Light intensity (mW/cm^2) (Z_2)	Rate constant (min^{-1}) (K')
1	72.25 (1)[c]	2.76 (1)	7.67×10^{-4}
2	72.25 (1)	1.14 (−1)	5.78×10^{-4}
3	22.75 (−1)	2.76 (1)	5.72×10^{-4}
4	22.75 (−1)	1.14 (−1)	5.61×10^{-4}
5	12.5 (−1.414)	1.95 (0)	6.76×10^{-4}
6	82.5 (1.414)	1.95 (0)	4.94×10^{-4}
7	47.5 (0)	0.8 (−1.414)	5.02×10^{-4}
8	47.5 (0)	3.1 (1.414)	1.40×10^{-3}
9	47.5 (0)	1.95 (0)	6.00×10^{-4}
10	47.5 (0)	1.95 (0)	5.88×10^{-4}
11	47.5 (0)	1.95 (0)	6.11×10^{-4}
12	47.5 (0)	1.95 (0)	6.33×10^{-4}
13	47.5 (0)	1.95 (0)	6.26×10^{-4}
14	47.5 (0)	1.95 (0)	6.83×10^{-4}
15	47.5 (0)	1.95 (0)	5.99×10^{-4}
16	47.5 (0)	1.95 (0)	7.06×10^{-4}

[a] Experiments were conducted in a random order.
[b] Mean values of triplicate determinations.
[c] Numbers in parentheses are coded symbols for levels of independent parameters as per the text.

to a second-order polynomial regression model (quadratic model) as shown in Eq. (4):

$$\hat{K}' = b_0 + \sum_{j=1}^{2} b_j x_j + \sum_{\substack{u,j=1 \\ u \neq j}}^{2} b_{uj} x_u x_j + \sum_{j=1}^{2} b_{jj} x_j^2 \quad (4)$$

where b_0 is constant and represented the value of the fitted response at the center of the design, b_j, b_{uj} and b_{jj} are linear, interaction and quadratic terms, respectively. The dimensionless x_j variable was used to reveal the coded variables corresponding to the studied parameters. The coded variables were obtained using the transforming Eqs. (5)–(7):

$$x_j = \frac{Z_j - Z_j^0}{\Delta Z_j}, \quad j = 1, 2 \quad (5)$$

$$Z_j^0 = \frac{Z_{j\,\max} + Z_{j\,\min}}{2}, \quad (6)$$

$$\Delta Z_j = \frac{Z_{j\,\max} - Z_j^0}{\gamma} \quad (7)$$

where x_j is the coded value of Z_j, $Z_{j\max}$ and $Z_{j\min}$, respectively represents the maximum and minimum levels of the factor j in natural units. Z_j^0 represents the value of Z_j at zero level and $\gamma = 1.414$. The coefficients of the fitted model were obtained using Eq. (8):

$$B = [X^T X]^{-1} [X]^T K' \quad (8)$$

where B is the column matrix for the estimated coefficients; $[X^T X]^{-1}$ represents the dispersion matrix; $[X]^T$ represents the transposed matrix of the experimental matrix[X] and K' represents the column matrix of the observations.

This design is a 2^2 factorial design (runs 1–4; see Table 2) and contained four axial points (runs 5–8) and eight replicates (runs 9–16, coded level 0). The axial points were positioned at the face of the cube portion based on the design that corresponded to a γ value of 1.414. The axial points and all replicates were added to the factorial design to provide the estimation of the model curvature and to allow for the estimation of experimental error [26].

The results of the CCRD experiments are tabulated in Table 2. Using the software program Excel, the model coefficients (Eq. (4)) were estimated using the least squares regression technique and Fischer's variance analysis (F-test) was carried out to test the statistical significance of the model.

Response surface and contour plots were developed using fitted polynomial equations to display the effects of the variables and were drawn using OrginLab7.5 software. When the results showed a saddle point in the response surface, optimal conditions were determined by analysis of the ridge. A subsequent confirmatory experiment was then carried out to validate the equation.

3. Results and discussion

3.1. Characterization of [TiO_2/ACF] and [TiO_2/ACF-Pt] electrode

SEM photographs of the original ACF and [TiO_2/ACF-Pt] supports are shown in Fig. 2. Comparing Fig. 2(a) with Fig. 2(b), it was found that there was little difference in the structure of ACF before and after preparation. This indicated that the microscopic structure of ACF was not damaged during preparation. The space between adjacent ACFs was sufficient to allow penetration of light or electrons into the felt-form photocatalyst to a particular depth; so that a three-dimensional environment was formed for the photocatalyst reaction [27]. It can be seen from Fig. 2(c) that there

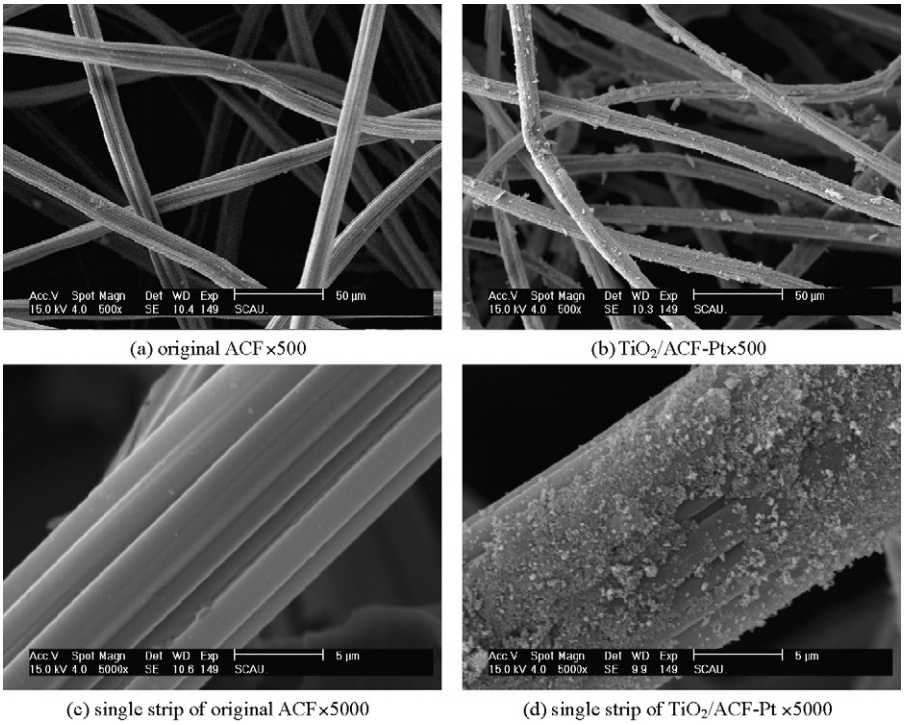

Fig. 2. SEM photographs of original ACF (a and c) and TiO_2/ACF-Pt (b and d).

were many long grooves on the surface of the original ACF. The images of TiO_2 immobilized on ACF-Pt are shown in Fig. 2(d). It can be seen that the TiO_2 particles have coagulated to form a large unit, i.e. TiO_2 clusters not thin-films, on the surface of ACF-Pt, and the distribution of the TiO_2 clusters on ACF-Pt was not uniform because of the fiber structure within the grooves and numerous micropores.

From the raw data of the nitrogen adsorption isotherms according to the Brunauer–Emmett–Teller (BET) methods, the specific surface areas (S_{BET}) of original ACF, TiO_2/ACF and TiO_2/ACF-Pt was 1231.7, 722.4 and 636 $m^2\,g^{-1}$, respectively. The S_{BET} of TiO_2/ACF and TiO_2/ACF-Pt were found to decline to different extents after TiO_2 or Ag + TiO_2 depositing. It implies that some of the pores of ACF were blocked by the TiO_2 or Ag + TiO_2 particles. Since the S_{BET} value was determined by the unit weight of ACF, [TiO_2/ACF] and [TiO_2/ACF-Pt], respectively, the TiO_2 or Ag + TiO_2 coverage in the electrode is not so high, indicating that certain amount of ACF's fibers was still exposed in the electrode. This phenomenon was also exhibited in Fig. 2(d). For the PC process, exposed ACF surfaces served as condensation centers for dilute substrates which were adsorbed on the surface; the condensed substrate would then be degraded by TiO_2 particles [28].

The surface morphology of the TiO_2 clusters on ACF and ACF-Pt were enlarged to a scale of using FESEM as shown in Fig. 3. The surface of TiO_2 clusters was composed of dispersed nanosized TiO_2 particles with rounded edges. Most of the particles were aggregated and a porous structure was formed. P25 TiO_2 served as a kind of pore wall as suggested by Chen and Dionysiou [29]. Both the pores of the TiO_2 clusters on ACF and ACF-Pt were similar, and the size of pores was observed to be between 20 nm and 80 nm. Inset of Fig. 3(b) displayed Pt particles having a "rice" shape or aggregates of less than 100 nm in the Pt deposited ACF initially (ACF-Pt). However, the Pt particles could not be distinguished from the TiO_2 particles in the TiO_2 clusters on ACF-Pt after TiO_2 loading; the reason for this may be that very few Pt particles were loaded onto the ACF and that the microscope resolution limited.

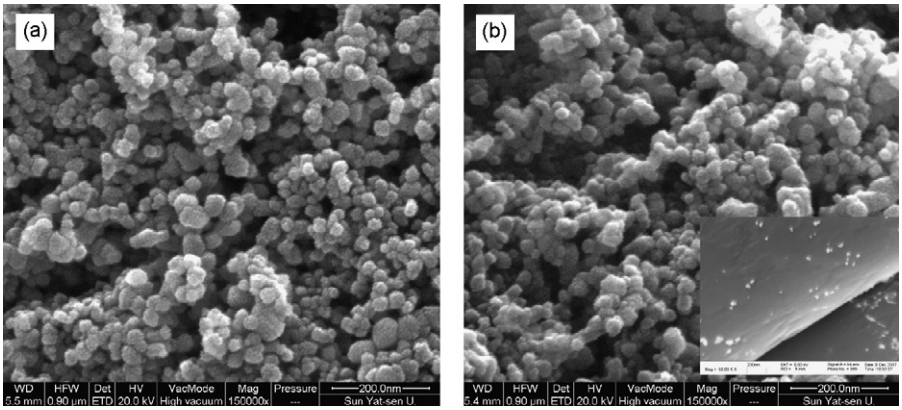

Fig. 3. FESEM analysis of surface morphology of (a) TiO_2 clusters on ACF ×150,000 and (b) TiO_2 clusters on ACF-Pt ×150,000, (inset) representation Pt deposited ACF initially ×50,000.

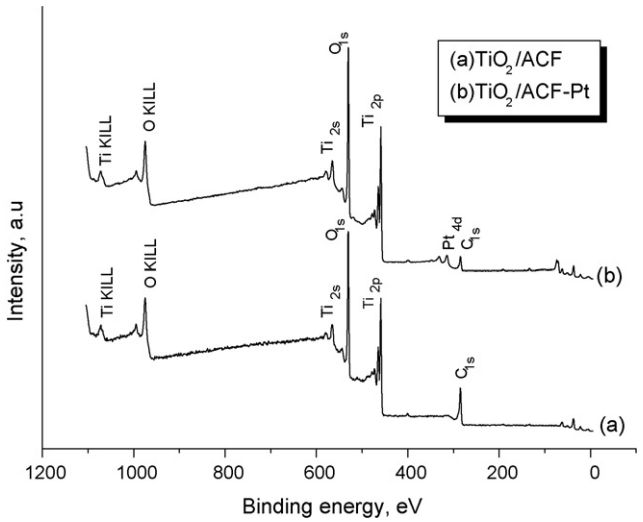

Fig. 4. The XPS survey scan spectrum of TiO_2/ACF and TiO_2/ACF-Pt.

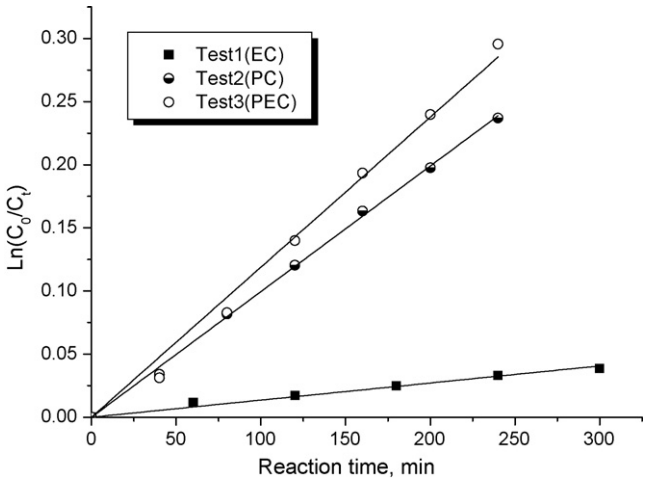

Fig. 5. Kinetics curves in the three processes.

XPS analysis gives a valuable insight into the surface structure of the electrode. The XPS survey scan spectrum of [TiO_2/ACF] and [TiO_2/ACF-Pt] is shown in Fig. 4. The spectra imply that the surface of both electrodes was mainly composed of elements: titanium dioxide, carbon and oxygen. All of these elements originate from the TiO_2 coating and ACF surface. In addition to the three elements, there was the Pt element on the surface of [TiO_2/ACF-Pt] as evidenced by the presence of the Pt peak. The surface atomic composition and concentration obtained by XPS analysis are shown in Table 3. The data indicated that the deposition of Pt on ACF initially decreased its carbon content and increased the O_{1s}/C_{1s} ratio. The phenomenon of decreased carbon content might be explained by the possibility that Pt anchorage resulted in a slight reduction in the surface area of ACF and in the micropore volume. However, deposition of Pt on ACF enhances the conductivity of the electrode.

3.2. Synergetic degradation of ethylene gas

Ethylene gas concentrations decreased in the PEC reactor with increasing reaction time. The kinetic curves of ethylene reduction in the three processes is presented in Fig. 5 with $\mathrm{Ln}(C_0/C_t) = K't$, and it should be noted that ethylene reduction was much slower in the dark (electrochemical, EC) process than in the PC and PEC processes, suggesting that efficient degradation of ethylene was not achieved using the EC process. The combination of UV irradiation and an applied potential accelerated the degradation process. The apparent rate constants for the processes of PEC, PC and EC using the [TiO_2/ACF] |Nafion|[TiO_2/ACF] assembly were $K'_{PEC} = 1.26 \times 10^{-3}$, $K'_{PC} = 9.95 \times 10^{-4}$ and $K'_{EC} = 1.35 \times 10^{-4}$ min^{-1}, respectively. The K' value of PEC was 1.26 and 9.33 times those in PC and EC processes, respectively. The $K'_{PEC}/(K'_{PC} + K'_{EC})$ value obtained from the above kinetic constants was 1.12. This confirmed that an apparent synergetic effect was observed in the PEC process.

The enhancement effect of the PEC process at a certain EMA voltage may be attributed to two factors. First, the external electric field can capture photogenerated electrons, reducing the recombination of these electrons and holes. Second, the external electric field can also cause electrochemical oxidation of ethylene in addition to the PEC synergetic effect. A key finding in the interpretation of the electrochemical promotion effect is the variation in the surface coverage and the work function of the electrode upon polarization, with concomitant changes in the binding strength of chemisorbed species and reaction intermediates [30].

Table 3
XPS data of atomic concentration on the surface of TiO_2/ACF and TiO_2/ACF-Pt.

	Atomic concentration (%)			
	C_{1s}	O_{1s}	Ti_{2p}	Pt_{4d}
TiO_2/ACF	45.26	39.42	13.77	0
TiO_2/ACF-Pt	21.74	56.57	19.51	2.18

3.3. Effect of applied electrical bias on the rate constant of ethylene degradation

Figs. 6 and 7 represent the rate constant (K') of the PEC processes in 240 min on the EMA [TiO_2/ACF] |Nafion| [TiO_2/ACF] and the EMA [TiO_2/ACF-Pt] |Nafion| [TiO_2/ACF-Pt] respectively at various applied electrical biases. Both insets in Figs. 6 and 7 illustrate that the plot of $\mathrm{Ln}(C_0/C_t)$ versus t resulted in straight lines with the regression coefficients (r^2) exceeding 0.98 in all cases. It can be seen from the figures that the two curves exhibit the following two differences.

Firstly, the apparent rate constant for PEC processes on the EMA of [TiO_2/ACF-Pt] |Nafion|[TiO_2/ACF-Pt] was higher than that of the EMA of [TiO_2/ACF] |Nafion| [TiO_2/ACF] in the range of applied voltages studied. This indicated that the enhancement effect of the external electric field in the presence of Pt was more obvious than that in the absence of Pt; the initially deposited Pt on ACF is beneficial to the PEC degradation of ethylene. This more obvious enhancement effect suggested that the deposited Pt not only traps

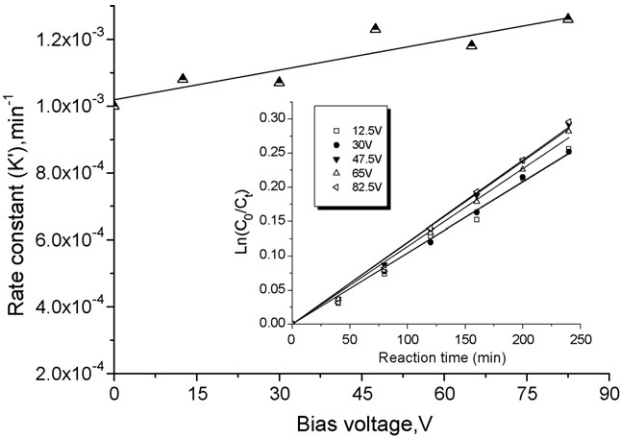

Fig. 6. Dependence of rate constant on electrical bias in [TiO_2/ACF] |Nafion| [TiO_2/ACF]. (Inset) Representation of $\mathrm{Ln}(C/C_0)$ vs. reaction time.

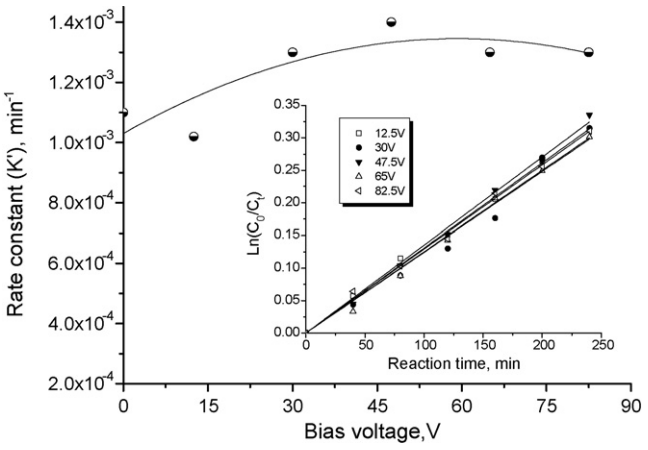

Fig. 7. Dependence of rate constant on electrical bias in [TiO_2/Pt-ACF] |Nafion| [TiO_2/Pt-ACF]. (Inset) Representation of $\mathrm{Ln}(C/C_0)$ vs. reaction time.

the photogenerated electrons but also assists migration of electrons in the external electric field.

Secondly, the two curves showed a different shape. With respect to PEC process on the EMA of [TiO_2/ACF] |Nafion| [TiO_2/ACF], the apparent rate constant increased linearly with increasing applied bias voltage. Compared with the rate constant in the PEC process on the EMA of [TiO_2/ACF-Pt] |Nafion| [TiO_2/ACF-Pt], the constant increases with increasing applied bias voltage below 47.5 V, and then, gradually decreases. There was a parabolic relationship between bias voltage and rate constant.

3.4. Predictive model of response and verification

The regression model of PEC on the EMA of [TiO_2/ACF-Pt] |Nafion| [TiO_2/ACF-Pt] for degradation of ethylene in the coded level of variables was predicted by Eq. (9) as follow:

$$\hat{K}' = 6.30 \times 10^{-4} - 5.67 \times 10^{-6}x_1 + 1.84 \times 10^{-4}x_2 + 4.45 \times 10^{-5}x_1x_2 - 5.95 \times 10^{-5}x_1^2 + 1.24 \times 10^{-4}x_2^2 \quad (9)$$

The results of the *F*-test for the reliability of the prediction equation are given in Table 4. As shown in Table 4, the F_1-ratio for the regression analysis of lack of fit was less than the critical *F* value for 3 and 7 degrees of freedom at the 99% confidence level, thus there was no evidence for a lack of fit. The regression equation was significant since the F_2-ratio of the regression significance was greater than the critical *F* value for 5 and 10 degrees of freedom at 95% confidence level. Thus, the response was sufficiently explained by the regression model. In order to express the effect of the bias voltage and light intensity more directly, Eqs. (5)–(7) are taken into Eq. (9). The final equation for the quadratic model of response (Eq. (10)) is as follow:

$$\hat{K}' = 8.99 \times 10^{-4} + 4.63 \times 10^{-6}Z_1 - 6.10 \times 10^{-4}Z_2 + 2.22 \times 10^{-6}Z_1Z_2 - 9.68 \times 10^{-8}Z_1^2 + 1.88 \times 10^{-4}Z_2^2 \quad (10)$$

The 3D graph of response surface and contour of the rate constant (K') versus bias voltage and light intensity is shown in Fig. 8. From this three-dimensional and contour plot, the effects of bias voltage and light intensity on the rate constant can be seen.

When the light intensity is higher than 2 mW cm^{-2}, the grade of response surface and the intervals along the contour lines were reduced in the direction of increasing light intensity. Light intensity plays an important role in influencing the rate constant. Studies suggest that the rate constant for the processes of PC can be a function of the square root of the light intensity [31] or a linear function of the light intensity [32]. From Fig. 7, it can be seen that it is better to use a quadratic polynomial formula to express the relationship between the apparent rate constant and the light intensity for the processes of PEC. Under the same light intensity above 2 mW cm^{-2}, when the bias voltage is below a specific value, e.g. 47.5 V bias voltage, the rate constant (K') increased with increasing applied electrical bias. This fact showed that an applied electrical bias for the EMA of [TiO_2/ACF-Pt] |Nafion|[TiO_2/ACF-Pt] provides enough bands bending to withdraw electrons, implying that the presence of Pt on TiO_2/ACF improves the conductivity of the film. When the bias voltage is above a specific value, the decrease in the rate constant is due to an electrochemical reaction of Pt, lessening amount of pure Pt on the ACF felt.

Table 4
The sum of squares variation and estimated *F* values for the least squares fit regression equation[a].

Source of variation	Sum of squares	Deg. freedom	Mean square
Regression	$SS_R = \sum_i^m \sum_j^{n_i} (\hat{K}'_i - \bar{K}')^2 = 4.29 \times 10^{-7}$	$p-1=5$	$MS_R = \frac{SS_R}{p-1} = 8.58 \times 10^{-8}$
Residual	$SS_r = \sum_i^m \sum_j^{n_i} (K'_{ij} - \hat{K}'_i)^2 = 2.28 \times 10^{-7}$	$n-p=10$	$MS_r = \frac{SS_r}{n-p} = 2.28 \times 10^{-8}$
Lack of fit	$SS_{lof} = \sum_i^m \sum_j^{n_i} (\hat{K}'_i - \bar{K}'_i)^2 = 2.15 \times 10^{-7}$	$m-p=3$	$MS_{lof} = \frac{SS_{lof}}{m-p} = 7.16 \times 10^{-8}$
Pure error	$SS_{pe} = \sum_i^m \sum_j^{n_i} (K'_{ij} - \bar{K}'_i)^2 = 1.33 \times 10^{-8}$	$n-m=7$	$MS_{pe} = \frac{SS_{pe}}{n-m} = 1.90 \times 10^{-9}$
Total	$SS_T = \sum_i^m \sum_j^{n_i} (K'_{ij} - \bar{K}')^2 = 6.57 \times 10^{-7}$	$n-1=15$	
$F_2 = \frac{MS_R}{MS_r} = 3.76 > F_{0.05}(5, 10)$	$F_1 = \frac{MS_{lof}}{MS_{pe}} = 37.59 < F_{0.0001}(3, 7)$		

[a] n_i: number of replicates at the *i*th level; *m*: number of distinct levels for the independent variables; $n = \sum n_i$: total number of observations; *p*: number of parameters in the model; $\hat{K}'_i$: the estimated value of rate constant for the *i*th observation; K'_{ij}: the observed value for rate constant of the *i*th observation.; $\bar{K}'$: the average value for the rate constant of the *i*th observation; $\bar{K}'_i$: the average value of the rate constant for the replicates.

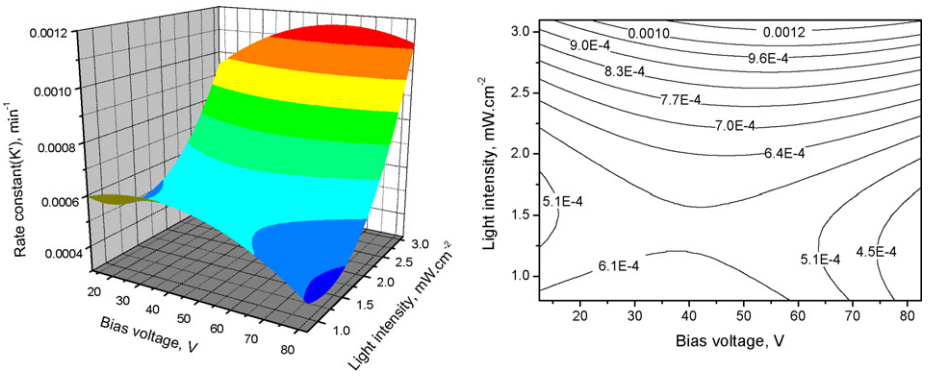

Fig. 8. Response surface plot and its contour plot showing effects of light intensity and bias voltage on rate constant.

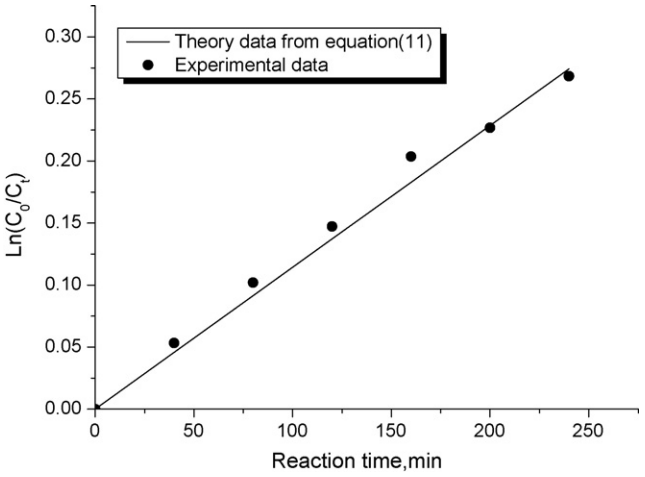

Fig. 9. A comparison of the estimated data using Eq. (11) with the experimental data under the conditions of light intensity (3.1 mW cm^{-2}) and bias voltage (47.5 V).

According to the canonical analysis described by Khuri and Cornell [33], the stationary points were located for the corresponding responses. In this study the search criteria were to obtain the highest apparent rate constant for the processes of PEC. Therefore, the optimum PEC conditions were established as 3.1 mW cm^{-2} and 47.5 V from ridge analysis, which correspond to the light intensity and the bias voltage, respectively. Based on Eq. (2), the PEC degradation processes of ethylene on the EMA of [TiO_2/ACF-Pt] |Nafion| [TiO_2/ACF-Pt] can be expressed by Eq. (11).

$$Ln\left(\frac{C_0}{C_t}\right) = (8.99\times10^{-4} + 4.63\times10^{-6}Z_1 - 6.10\times10^{-4}Z_2 + 2.22\times10^{-6}Z_1Z_2 - 9.68\times10^{-8}Z_1^2 + 1.88\times10^{-4}Z_2^2)t \quad (11)$$

In order to check the accuracy of Eq. (11), the theoretical data was compared with the experimental data using Eq. (11) under the conditions of light intensity = 3.1 mW cm^{-2} and the bias voltage = 47.5 V, when the initial concentration = 45.5 mg m^{-3}. The experimental results shown in Fig. 9 demonstrated that the estimated value of $Ln(C_0/C_t)$ is slightly lower than the experimental data when the irradiation time is less than 150 min. The t value based on 7 differences between the theoretical data from Eq. (11) and the experimental data yields −1.71, and then the P-value is 0.138. Therefore, the experimental data were in perfect agreement with the calculated data, which confirms the adequacy of Eq. (11).

In this section we modeled the relationship between the rate constant (K') and the affecting parameters of PEC reactor under a simulated cold environment inside an ethylene-sensitive produce storage. Yamazaki et al. [34] reported that the reaction rate of photo-assisted catalytic degradation of ethylene was influenced by parameters of PC reactor such as light intensity, in addition to process variables and environmental factors such as the initial ethylene concentration, temperature, water vapor and oxygen. Temperature requirements, which can range from 0.5 to 10 °C, may necessitate several different storage environments. Similarly, humidity requirements range from 85% to 100% except for a few products such as onions, which require low humidity. Therefore process variables and environmental factors of PEC degradation of ethylene other than designing parameters of PEC reactor will need to be taken into account for the future modeling, in particular the initial ethylene concentration. However, since the presented model can identify the quantitative estimation of the key designing parameters of PEC reactor, it may assist our understanding of PEC degradation of ethylene and fabricating PEC reactor with higher efficiency for the next extensive experiments.

4. Conclusions

The experiment demonstrated Photoelectrocatalysis using an ACF-supported photocatalyst TiO_2 photoelectrode [TiO_2/ACF] or a photoelectrode comprising the photocatalyst TiO_2 supported on ACF modified by the deposition of platinum [TiO_2/ACF-Pt] can degrade ethylene at a temperature of 3 ± 1 °C temperature and relative humidity of 90 ± 3%. The degradation of ethylene by applying bias voltage on the EMA of [TiO_2/ACF] |Nafion| [TiO_2/ACF] or on the EMA of [TiO_2/ACF-Pt] |Nafion| [TiO_2/ACF-Pt] enhanced the efficiency of PC degradation in terms of the rate constant of the apparent pseudo-first-order kinetic model. The combination of ACF modified by deposited platinum and applied bias voltage have an additive enhancement effect on the rate constant compared to PEC degradation without Platinum deposition on ACF. With respect to the EMA of [TiO_2/ACF-Pt] |Nafion| [TiO_2/ACF-Pt], a kinetic model was established to describe the relationship between the rate constant and the affecting factors. Optimized parameters were found to be a light intensity of 3.1 mW cm^{-2} with a bias voltage of 47.5 V.

Acknowledgements

Financial support from the National Natural Science Foundation of China (30571075 and 30871446) and the Natural Science Foundation of Guangdong Province, China (8151064201000032) is gratefully acknowledged by the authors.

References

[1] F.B. Abeles, P.W. Morgan, M.E. Saltveit, Ethylene in Plant Biology, second ed., Academic Press, San Diego, 1992.

[2] T.K. Graham, J.N. Veenstra, P.R. Armstrong, Ethylene removal in fruit and vegetable storages using a plasma reactor, Trans. ASAE 41 (1998) 1767–1773.
[3] T.N. Obee, S.O. Hay, Effect of moisture and temperature on the photooxidation of ethylene on titania, Environ. Sci. Technol. 31 (1997) 2034–2038.
[4] T.W. Tibbitts, K.E. Cushman, X. Fu, M.A. Anderson, R.J. Bula, Factors controlling activity of zirconia–titania for photocatalytic oxidation of ethylene, Adv. Space Res. 22 (1998) 1443–1451.
[5] D.R. Park, J.L. Zhang, K. Ikeue, H. Yamashita, M. Anpo, Photocatalytic oxidation of ethylene to CO_2 and H_2O on ultrafine powdered TiO_2 photocatalysts in the presence of O_2 and H_2O, J. Catal. 185 (1999) 114–119.
[6] K. Surajit, G.F. Andrei, L.G. James, Photodegradation of ethylene using visible light responsive surfaces prepared from titania nanoparticle slurries, Appl. Catal B: Environ. 57 (2005) 93–107.
[7] C. Maneerat, Y. Hayata, N. Egashira, K. Sakamoto, Z. Hamai, M. Kuroyanagi, Photocatalytic reaction of TiO_2 to decompose ethylene in fruit and vegetable storage, Trans. ASAE 46 (2003) 725–730.
[8] J.M. Herrmann, Heterogeneous photocatalysis fundamentals and applications to the removal of various types of aqueous pollutants, Catal. Today 53 (1999) 115–129.
[9] A.W. Xu, Y. Gao, H.Q. Liu, The preparation, characterization, and their photocatalytic activities of rare-earth-doped TiO_2 Nanoparticles, J. Catal. 207 (2002) 151–376.
[10] T.A. Egerton, P.A. Christensen, Photoelectrocatalysis process, in: S. Parsons (Ed.), Advanced Oxidation Process for Water and Wastewater Treatment, IWA Publishing, London, 2004.
[11] P.A. Carneiro, M.E. Osugi, J.J. Sene, M.A. Anderson, M.V.B. Zanoni, Evaluation of color removal and degradation of a reactive textile azo dye on nanoporous TiO_2 thin-film electrodes, Electrochim. Acta 49 (2004) 3807–3820.
[12] M. Hepel, S. Hazelton, Photoelectrocatalytic degradation of diazo dyes on nanostructured WO_3 electrodes, Electrochim. Acta 50 (2005) 5278–5291.
[13] C. He, Y. Xiong, D. Shu, X. Zhu, X. Li, Preparation and photoelectrocatalytic activity of Pt (TiO_2)–TiO_2 hybrid films, Thin Solid Films 503 (2006) 1–7.
[14] P.A. Christensen, T.A. Egerton, S.A.M. Kosa, J.R. Tinlin, K. Scott, The photoelectrocatalytic oxidation of aqueous nitrophenol using a novel photoelectrochemical reactor, J. Appl. Electrochem. 35 (2005) 683–692.
[15] T. An, Y. Xiong, G. Li, X. Zhu, G. Sheng, J. Fu, Improving ultraviolet light transmission in a packed-bed phtoelectrocatalytic reactor for removal of oxalic acid from wastewater, J. Photochem. Photobiol. A: Chem. 181 (2006) 158–165.
[16] L.C. Macedo, D.A.M. Zaia, G.J. Moore, H.de. Santana, Degradation of leather dye on TiO_2: A study of applied experimental parameters on photoelectrocatalysis, J. Photochem. Photobiol. A: Chem. 185 (2007) 86–93.
[17] J.Q. Li, L. Zheng, L.P. Li, Y. Xian, L. Jin, Fabrication of TiO_2/Ti electrode by laser-assisted anodic oxidation and its application on photoelectrocatalytic degradation of methylene blue, J. Hazard. Mater. (139) (2007) 72–78.
[18] T.A. Egerton, M. Janus, A.W. Morawski, New TiO_2/C sol–gel electrodes for photoelectrocatalytic degradation of sodium oxalate, Chemosphere 63 (2006) 1203–1208.
[19] R. Hopmen, W.G. Siegers, J.C. Kruithof, Organic micropollutant removal by activated carbon fiber filtration, Water Supply 13 (1995) 257–261.
[20] R.C. Bansal, J.B. Donnet, F. Stoeckli, Active Carbon, Marcel Dekker, New York, 1988.
[21] C.M. Yang, K. Kaneko, Adsorption properties of iodine-doped activated carbon fiber, J. Colloid. Interf. Sci. 246 (2002) 34–39.
[22] R.B. Sun, Z.G. Xi, F.H. Chao, W. Zhang, H.S. Zhang, D.F. Yang, Decomposition of low-concentration gas-phase toluene using plasma-driven photocatalyst reactor, Atmos. Environ. 41 (2007) 6853–6859.
[23] T. Guo, Z.P. Bai, C. Wu, T. Zhu, Influence of relative humidity on the photocatalytic oxidation (PCO) of toluene by TiO_2 loaded on activated carbon fibers: PCO rate and intermediates accumulation, Appl. Catal. B: Environ. 79 (2008) 171–178.
[24] S.R.de. Miguel, J.I. Vilella, E.L. Jablonski, O.A. Scelza, Preparation of Pt catalysts supported on activated carbon felts (ACF), Appl. Catal A: Gen. 232 (2002) 237–246.
[25] J.Y. Wang, F.Y. Zhao, Y.Q. Hu, R.H. Zhao, R.J. Liu, Modification of activated carbon fiber by loading metals and their performance on SO_2 removal, Chin. J. Chem. Eng. 14 (2006) 478–485.
[26] G.E.P. Box, J.S. Hunter, W.G. Hunter, Statistics for Experiments, fourth ed., Wiley-Interscience, New York, 2005.
[27] P. Fu, Y. Luan, X. Dai, Preparation of TiO_2 photocatalyst anchored on activated fibers and its photodegradation of methylene blue, Chin. Particuol. 2 (2004) 76–80.
[28] H. Yamashita, Y. Ichihashi, M. Harada, G. Stewart, M.A. Fox, M. Anpo, Photocatalytic degradation of 1-octanol on anchored titanium oxide and on TiO_2 powder catalysts, J. Catal. 158 (1996) 97–101.
[29] Y.J. Chen, D.D. Dionysiou, Bimodal mesoporous TiO_2–P25 composite thick films with high photocatalytic activity and improved structural integrity, Appl. Catal. B: Environ. 80 (2008) 147–155.
[30] C.G. Vayenas, S. Bebelis, I.V. Yentekakis, H.-G. Lintz, Non-faradaic electrochemical modification of catalytic activity: A status report, Catal. Today 11 (1992) 303–438.
[31] D. Bahnemann, D. Bocklmann, R. Goslich, Mechanistic studies of water detoxification on illuminated TiO_2 suspension, Solar Energy Mater. 24 (1991) 564–568.
[32] M.W. Peterson, J.A. Turner, A.J. Nozik, Mechanistic studies of the photocatalytic behavior of titania: particles in a photoelectrochemical slurry cell and the relevance to photodetoxification reactions, J. Phys. Chem. 95 (1991) 221–225.
[33] A.A. Khuri, J.A. Cornell, Response Surface: Design and Analyses, Marcel Dekker, New York, 1987.
[34] S. Yamazaki, S. Tanaka, H. Tsukamoto, Kinetic studies of oxidation of ethylene over a TiO_2 photocatalyst, J. Photochem. Photobiol. A: Chem. 121 (1999) 55–61.